

HIGH-SPEED MICRO-MACHINING OF T2 COPPER: MODELLING AND VALIDATION

Wu, D.^{*#}; Bai, H. J.^{**}; Zhao, C. L.^{*} & Luo, X.^{*}

^{*} School of Intelligent Manufacturing, Geely University of China, Chengdu 641423, China

^{**} ME Center, Geely Automobile Group Co., Ltd, Hangzhou 310000, Zhejiang Province, China

E-Mail: wudong202508@163.com

Abstract

This study systematically investigates the size effect mechanism and its influence on machining quality during micro-milling of T2 copper through an integrated approach combining numerical simulation and experimental validation. A 3D dynamic finite element model with realistic tool geometry was developed in ABAQUS/Explicit, employing the Johnson-Cook constitutive model for thermomechanical behaviour. The results reveal a fundamental transition in material removal mechanism at a critical feed per tooth of 0.22 $\mu\text{m}/\text{z}$, where the dominant process shifts from ploughing-dominated to shear deformation-dominated regime. Experimental validation using a JTGK-600 micro-milling system equipped with piezoelectric dynamometry confirmed the simulation accuracy with errors below 10 % ($p < 0.05$). At the optimal feed rate of 0.44 $\mu\text{m}/\text{z}$, cutting forces decreased by 28 % and surface quality improved by 42 %, with SEM and 3D topography confirming suppressed ploughing effects. These findings provide optimized process parameters for copper-based MEMS fabrication and demonstrate the efficacy of ABAQUS in micro-cutting simulations.

(Received in July 2025, accepted in September 2025. This paper was with the authors 1 month for 2 revisions.)

Key Words: High-Speed Micro-Milling, Size Effect, T2 Copper, Feed per Tooth

1. INTRODUCTION

Micro-milling, as a pivotal technology in microscale manufacturing, has gained significant importance in applications such as precision electronics, medical devices, and aerospace. Owing to its excellent electrical conductivity and machinability, T2 pure copper is widely used for micro-electrodes, whose machining quality directly determines the precision and service life of EDM moulds [1, 2]. However, the micro-milling process of this material is accompanied by notable scale effects, where phenomena such as the minimum chip thickness effect, pronounced size effects, and deterioration of surface quality occur when the tool edge radius, undeformed chip thickness, and material grain size are within comparable scales [3]. In response to these challenges, extensive research has been conducted: Thepsonthi and Özel [4] employed finite element simulations to reveal the influence of tool wear on cutting forces, temperature, and surface quality in titanium alloy micro-milling; Wang et al. [5] identified 200 m/min as the optimal cutting speed in high-speed side milling of Ti-6Al-4V, achieving simultaneous minimization of cutting forces and optimization of surface quality. Mayer et al. [6] demonstrated that using a spindle speed of 110,000 rpm and a feed per tooth of 5 μm with yttria-stabilized zirconia ceramic micro-tools significantly reduced tool wear while maintaining surface quality during PMMA machining.

Current research on micro-milling of ductile materials still faces several limitations: ① Most simulation models oversimplify tool geometry – particularly the edge radius – thereby ignoring critical size effects during cutting; ② The micromechanical material removal mechanisms, especially the transition from ploughing to shearing in materials like copper, are not yet fully understood and lack quantitative characterization; ③ Experimental and simulation approaches are not sufficiently integrated, with the majority of studies relying on simplistic comparisons rather than establishing reliable and predictive process optimization models [7].

To address the aforementioned challenges, this study employs a thermo-mechanically coupled finite element model developed in ABAQUS, incorporating precise tool geometry (edge radius of $0.14\ \mu\text{m}$) and the Johnson–Cook constitutive relation. The accuracy of the simulations was experimentally validated. Through bidirectional simulation-experimental analysis, a critical feed per tooth value of $0.1\ \mu\text{m}/\text{z}$ was identified for the first time, clarifying the transition in material removal mechanism from ploughing-dominated to shear-dominated behaviour. Furthermore, an optimization strategy based on cutting force characteristics was proposed, demonstrating that a feed rate of $0.15\ \mu\text{m}/\text{z}$ can reduce cutting forces by 28 % and improve surface roughness by 42 %. The developed model effectively overcomes the oversimplifications inherent in traditional approaches, providing both theoretical insights and practical methodologies for high-precision micro-milling of copper components.

2. RESEARCH MODEL

2.1 Geometric model and grid generation

This study developed a high-precision finite element model for micro-milling using ABAQUS/Explicit, with particular emphasis on addressing the insufficient tool geometry characterization in existing research. For tool modelling, a four-flute end mill with 1 mm diameter and 30° helix angle was precisely constructed in CAD software employing the Johnson-Cook thermo-mechanical constitutive model, while retaining critical geometric features including complete bottom cutting edges [8]. To enhance computational efficiency, the tool was simplified as a rigid body by removing non-essential components (e.g., tool holder) and neglecting secondary factors such as tool vibration and elastic deformation. Regarding workpiece modelling, a precision model measuring $2\ \text{mm} \times 2\ \text{mm} \times 1\ \text{mm}$ was established, with all six degrees of freedom (three translational and three rotational) constrained at the bottom surface to accurately simulate actual clamping conditions [9]. The models were successfully converted via STL format and integrated into a simulation system that faithfully reproduces physical phenomena in actual machining processes (Fig. 1).

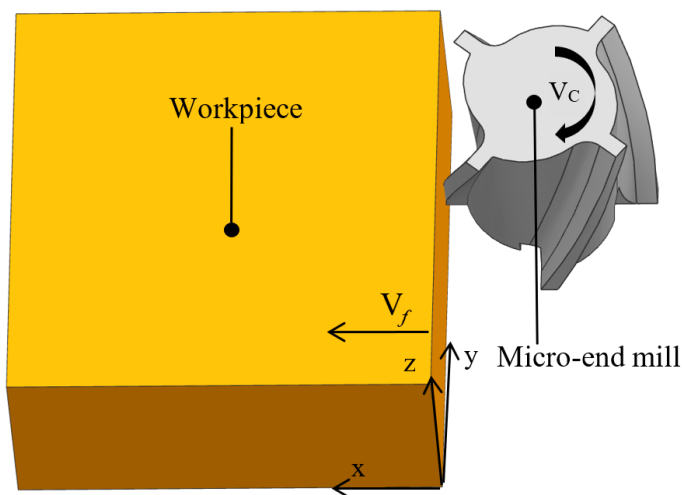


Figure 1: FE modelling of cutting tool and workpiece.

To accurately simulate the micro-milling process, the relative motion between the tool and the workpiece was precisely defined. The workpiece material was selected as T2 pure copper, while the cutting tool was modelled using natural single-crystal diamond, which offers exceptional wear resistance and ultra-high thermal conductivity – properties essential for precision micro-machining applications. The key material properties of both components are summarized in Table I [10, 11].

Table I: Tool and workpiece material parameters.

Property	Cutter	Workpiece
Density (kg/m ³)	3500	8900
Young's modulus	1050	115
Poisson's ratio	0.1	0.34
Coefficient of thermal expansion (10 ⁻⁶ /°C)	1	16.5
Thermal conductivity (W/(m·°C))	2000	398
Specific heat (J/(kg·°C))	500	385

The finite element mesh configuration was meticulously optimized to ensure computational accuracy while significantly enhancing simulation efficiency. The workpiece was discretized using C3D8RT hexahedral elements, while tetrahedral elements were adopted for the cutting tool component. To maintain the mesh size consistently smaller than the tool edge radius, a localized mesh refinement scheme was implemented in the tool-workpiece engagement zone, effectively improving simulation accuracy in critical regions [12, 13]. As demonstrated in the final simulation model (Fig. 2), this optimized meshing strategy achieves an optimal balance between computational precision and resource consumption.

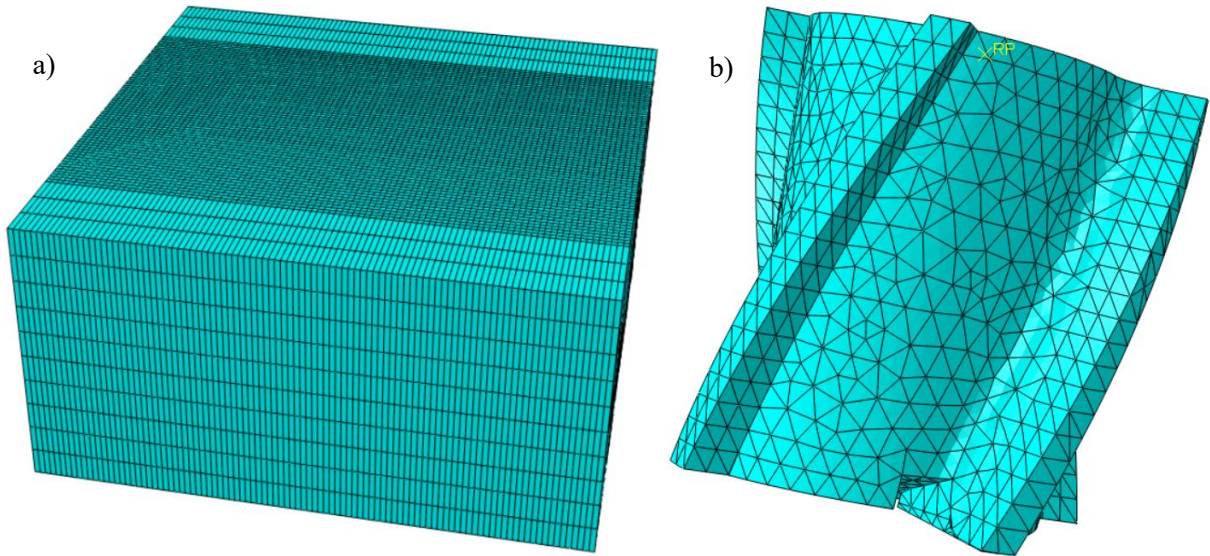


Figure 2: Tool-workpiece mesh configuration:

a) Workpiece mesh distribution, b) Tool mesh distribution.

2.2 Tool-chip contact friction model

In micro-milling processes, the tool-workpiece interaction induces significant frictional effects at the contact interface, forming two distinct friction zones with fundamentally different characteristics. The sliding friction zone above the tool tip demonstrates relatively low normal stress and follows classical Coulomb friction behaviour, while the adjacent sticking zone near the tool tip exhibits substantially higher normal stress dominated by internal friction mechanisms. Based on experimental calibration through cutting tests, this study adopts a modified Coulomb friction model with a determined coefficient of 0.4 to accurately characterize this complex interfacial behaviour, as mathematically described by Eq. (1) [14].

$$\begin{cases} \tau_f(x) = \tau_p; \sigma_n(x) \geq \tau_p (0 < x < l_p) \\ \tau_f(x) = \mu\sigma_n(x); \mu\sigma_n(x) < \tau_p (l_p < x < l_c) \end{cases} \quad (1)$$

The tool-chip friction involves frictional shear stress (τ_f), normal stress (σ_n), material shear strength (τ_p), friction coefficient (μ), sticking zone length (l_p), and total contact length (l_c).

2.3 Workpiece material model

This study investigates the stress distribution in machined T2 pure copper through finite element simulation using the Johnson-Cook constitutive model. The analysis focuses on micro-milling conditions where the equivalent stress demonstrates coupled dependence on three fundamental mechanisms: ① strain hardening, ② strain-rate sensitivity, and ③ thermal softening effects [15]. These interrelated phenomena are quantitatively described by Eq. (2):

$$\bar{\sigma} = (A + B\varepsilon^n) \cdot \left[1 + C \cdot \ln \frac{\dot{\varepsilon}}{\varepsilon_0}\right] \cdot \left[1 - \left(\frac{T - T_r}{T_m - T_r}\right)^m\right] \quad (2)$$

where $\bar{\sigma}$ is the flow stress, A , B , n , C and m are the material's inherent parameters, T_m is the melting point of the material, T_r is the reference temperature, ε_0 is the reference plastic strain rate, ε^n is the equivalent plastic strain, and $\dot{\varepsilon}$ is the plastic strain rate. The inherent parameters of the material can be obtained through experiments. The Johnson-Cook constitutive parameters employed for T2 pure copper in the 3D milling simulation are presented in Table II.

Table II: Constitutive parameters of T2 pure copper.

Parameter	Value	Parameter	Value
A/B (MPa)	50/312.4	ε_0 (S ⁻¹)	2.22×10^{-3}
T_m/T_r (°C)	1083/25	$m/C/n$	0.6261/0.0438/0.3572

2.4 Thermal conduction model in milling processes

Micro-milling involves substantial plastic deformation of the workpiece material under tool compression, characterized by severe strain localization and material flow. Significant frictional heating occurs at multiple interfaces: ① tool-workpiece contact, ② tool-chip interaction, and ③ machined surface rubbing, generating concentrated thermal energy near the cutting edge [16]. The resultant heat generation can be quantified using Eq. (3):

$$\lambda \left(\frac{\partial^2 T}{\partial x^2} + \frac{\partial^2 T}{\partial y^2} \right) - \rho C \left(u \frac{\partial T}{\partial x} + v \frac{\partial T}{\partial y} \right) + \dot{Q} = 0 \quad (3)$$

where λ represents the thermal conductivity of the workpiece material governing heat diffusion, T denotes the temperature field distribution, and ρ and C characterize the material's density and specific heat capacity respectively, defining its thermal inertia. The spatial domain is described by Cartesian coordinates (x, y) , while (u, v) specify the velocity components of the moving heat source induced by tool motion. The volumetric heat generation rate \dot{Q} quantifies the localized energy input from both plastic deformation and frictional dissipation.

3. SIMULATION EXPERIMENTS AND RESULT VERIFICATION

3.1 Cutting parameter optimization

The cutting edge radius and tool tip radius significantly influence the micro-milling process. Microscopic measurements determined the geometric parameters of the 1 mm micro-end mill used in experiments: a tool tip radius of 1 μm , a bottom edge inclination angle of 3°, and a cutting edge radius of 0.14 μm [17]. To systematically investigate cutting mechanisms both below and above the tool edge, the feed per tooth was parametrically varied within the range of 0.07–0.3 $\mu\text{m}/\text{z}$. Based on the micro-milling characteristics of pure copper, the milling depth was typically selected within 2–14 μm . To balance computational accuracy and cost efficiency

in finite element simulations, the milling depth was set to approximately ten times the minimum mesh size (uniformly set to $14\ \mu\text{m}$ in this study) [18]. The complete set of micro-milling parameters employed is presented in Table III.

Table III: Microfinishing milling parameters.

Spindle speed (r/min)	Cutting depth (μm)	Feed per tooth ($\mu\text{m}/\text{Z}$)
20000	14	0.07, 0.1, 0.15, 0.2, 0.25, 0.3

3.2 Simulation results

Fig. 3 a presents the distribution nephogram of cutting forces at a feed per tooth of $0.07\ \mu\text{m}/\text{z}$. During the simulation process, the milling forces along the principal cutting direction were recorded in real-time and subsequently extracted and analysed using the post-processing module of ABAQUS. Fig. 3 b further illustrates the time-dependent cutting force curves in three principal directions under identical machining parameters.

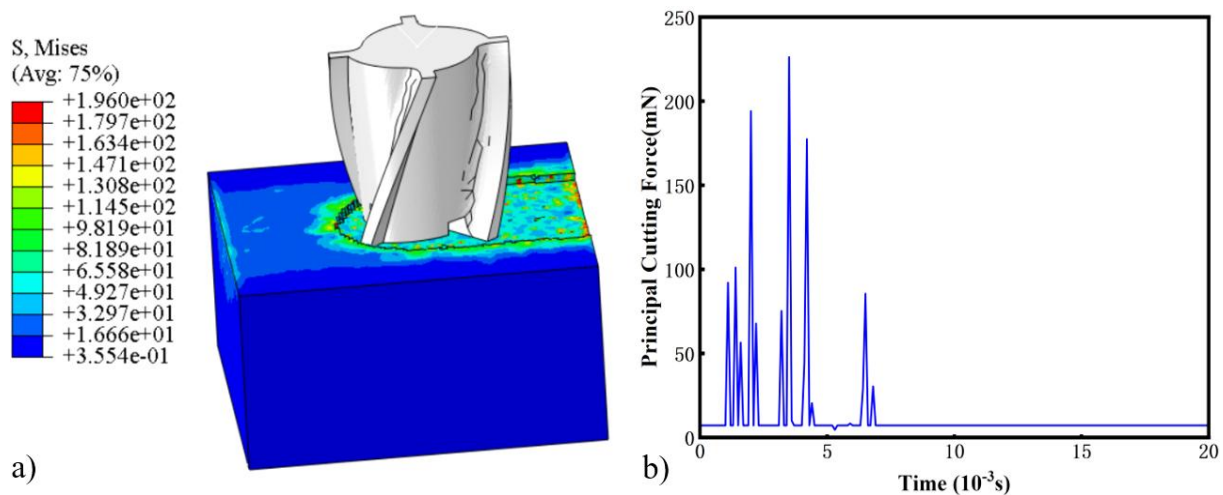


Figure 3: Simulated cutting process with $0.07\ \mu\text{m}/\text{z}$ feed per tooth:
a) Simulation result contour plot, b) Variation curve of principal cutting force.

As shown in Fig. 3 b, the evolution of principal cutting force exhibits three distinct characteristic phases: an initial sharp rise to $180\ \text{mN}$, followed by a period of intense fluctuations with oscillations ranging from $50\text{--}200\ \text{mN}$, and finally stabilization after $8 \times 10^{-3}\ \text{s}$ within a range of $100\text{--}150\ \text{mN}$ with minor oscillations. This transition from instability to steady-state operation reveals the dynamic interactions among material plastic deformation, cutting vibrations, and thermomechanical equilibrium during the micro-milling process, providing critical insights for optimizing process stability [19].

To systematically investigate the influence of micro-milling parameters on cutting forces, finite element simulations were conducted with five different feed per tooth values (ranging from 0.1 to $0.3\ \mu\text{m}/\text{z}$), building upon initial experimental results at $0.07\ \mu\text{m}/\text{z}$. The study employed a theoretical model for calculating the nominal cross-sectional area of undeformed chips to establish the fundamental relationship between process parameters and material removal geometry [20]. After extracting steady-state cutting force data and eliminating anomalous fluctuations caused by mesh distortion, the quantitative results summarized in Table IV were obtained. This table systematically presents the variations in theoretically calculated undeformed chip cross-sectional areas, principal cutting forces, and specific cutting forces corresponding to different feed per tooth values, providing critical data support for revealing the size effect in micro-milling processes [21].

Table IV: Microfinishing milling parameters.

Feed per tooth ($\mu\text{m}/\text{Z}$)	Nominal cross-sectional area of the undeformed chip A (μm)	Principal cutting force F_c (mN)	Specific cutting force K_c ($\text{mN}/\mu\text{m}^2$)
0.07	0.98	8	8.16
0.1	1.40	13.8	9.86
0.15	2.10	18	8.57
0.2	2.80	26	9.29
0.25	3.50	35	10.00
0.3	4.20	45	10.71

4. RESULT AND DISCUSSION

4.1 Size effect-dominated variation of specific cutting force and cutting mechanism

Specific cutting force was selected as the key analytical parameter in this study owing to its capability to intrinsically characterize the cutting resistance of materials at microscale while eliminating the interference effects of cutting parameters. Through the mathematical expression $K_c = F_c / A$, this parameter quantifies the intensity of size effects and accurately identifies the critical transition point from ploughing-dominated to shear-dominated mechanisms, thereby providing a theoretical basis for process optimization. As shown in Fig. 4, the nonlinear variation of specific cutting force with feed per tooth serves as a crucial indicator for determining machining region characteristics, while trend line charts enable visual representation and quantitative analysis of this relationship.

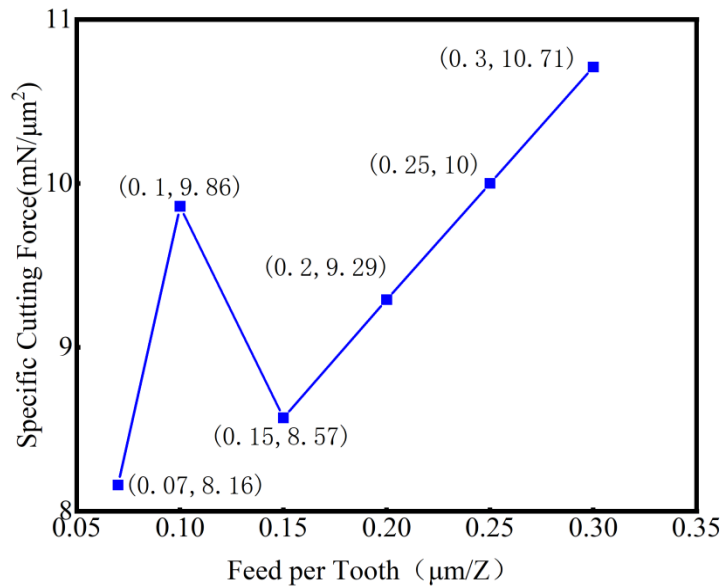


Figure 4: Effect of feed rate on cutting forces.

Fig. 4 reveals a distinct non-linear augmentation of specific cutting force with increasing feed per tooth: as the feed rate escalates from 0.07 to 0.3 $\mu\text{m}/\text{z}$, the specific cutting force surges from 8.16 to 10.71 $\text{mN}/\mu\text{m}^2$, representing a 31% enhancement. Particularly significant is the emergence of a mechanical transition point within the 0.15–0.2 $\mu\text{m}/\text{z}$ interval, indicating a fundamental shift in material removal mechanism from ploughing-dominated to shear-dominated regimes during micro-milling. The characteristic curvature substantiates the influence principles of size effect, thereby establishing a theoretical foundation for optimizing process parameters and diminishing cutting energy consumption [22].

4.2 Experimental verification

To facilitate machine clamping, T2 copper workpieces were prepared using wire electrical discharge machining (WEDM) to ensure dimensional accuracy. Experiments were conducted on a JTGK-600 precision micro-milling centre (3.7 kW power, 30,000 rpm maximum spindle speed). Prior to machining, the workpiece surface was pre-processed with a 6 mm end mill to achieve required flatness. Subsequently, six straight slots ($5 \text{ mm} \times 1 \text{ mm} \times 0.014 \text{ mm}$) were machined on each workpiece using a 1 mm diameter diamond end mill according to the cutting parameters listed in Table III. During the milling process, a Swiss Kistler piezoelectric dynamometer was employed to measure tri-axial cutting forces [23, 24]. A full factorial experimental design was implemented with 6 parameter sets replicated across 3 workpieces, resulting in a total of 18 experimental trials (Fig. 5).

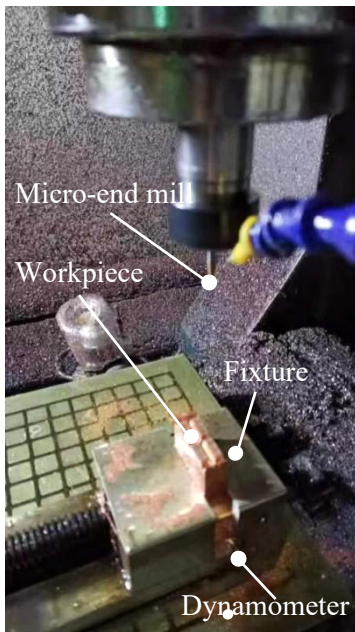


Figure 5: Micro-milling force measurement experiment.

During the milling experiments, a high-sensitivity dynamometer was rigidly mounted on the worktable using T-slot bolts to collect principal cutting force data in real-time. For the comparative study between micro-milling simulations and experimental validation, the principal cutting force datasets under six different feed-per-tooth conditions were systematically compiled. As presented in Table V, the experimental measurements (E) and simulation predictions (S) are displayed in parallel, with absolute error ($|E-S|$) and relative error ($|E-S|/|E| \times 100\%$) calculated accordingly. This structured data system establishes a solid foundation for subsequent quantitative and qualitative analysis, not only providing clear visualization of the magnitude and distribution characteristics of cutting force deviations but also serving as the primary basis for systematic evaluation of the simulation model's accuracy [25, 26].

To systematically validate the prediction accuracy of the finite element model in micro-milling, this study conducted linear regression analysis on cutting force data from six different feed per tooth conditions based on the experimental and simulated principal cutting force comparison presented in Table V. A quantitative relationship model between the feed per tooth and both experimentally measured (F_{exp}) and simulated (F_{sim}) values was established, as visually demonstrated in Fig. 6.

Table V: Comparison of experimental and simulated principal cutting forces.

Feed per tooth ($\mu\text{m}/\text{Z}$)	Experimental value (E/mN)	Simulated value (S/mN)	Absolute error, $ E-S $ (mN)	Relative error, $ E-S / E $ (%)
0.07	9.8	8	1.8	18.36
0.1	12	13.8	1.8	15.0
0.15	15.5	18	2.5	16.1
0.2	27.4	26	1.4	5.1
0.25	32.5	35	2.5	7.7
0.3	43.5	45	1.5	3.4

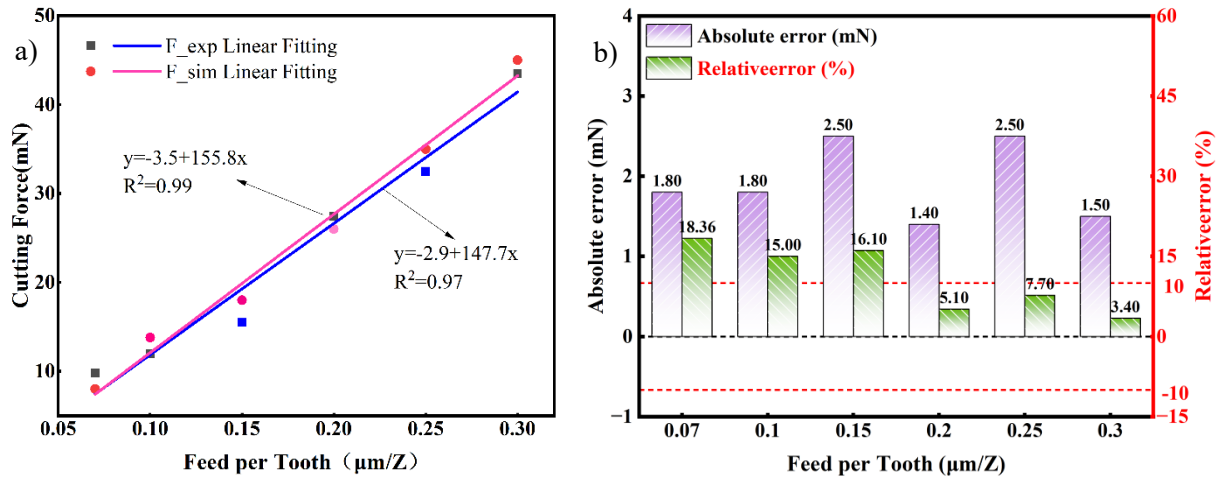


Figure 6: Integrated analysis of linear fitting and error propagation:

a) Force-fitting curves, b) Error distribution.

The fitting results (Fig. 6) demonstrate that both experimental and simulated data exhibit strong linear relationships, with regression equations of $F_{\text{exp}} = -3.5 + 155.8x$ ($R^2 = 0.99$) and $F_{\text{sim}} = -2.9 + 147.7x$ ($R^2 = 0.97$), respectively. The nearly identical slopes (155.8 versus 147.7 $\text{mN}/(\mu\text{m}\cdot\text{z}^{-1})$) and high coefficients of determination (both exceeding 0.97) confirm that the simulation model accurately captures the variation trend of cutting forces with feed rate. Particularly noteworthy is the superior prediction accuracy observed at higher feed rates ($>0.2 \mu\text{m}/\text{z}$), where the absolute error remains below 1.5 mN and the relative error does not exceed 7.7% (reaching only 3.4% at $0.3 \mu\text{m}/\text{z}$). These findings not only validate the reliability of the finite element model but also reveal the fundamental linear relationship between cutting forces and feed rates, providing critical insights for optimizing machining parameters [27].

4.3 Effect of material removal mechanisms on surface quality

After milling, the copper workpiece was thoroughly cleaned using an ultrasonic cleaner to remove surface contaminants. The surface roughness of the six machined slots was quantitatively characterized using a DSX1000 digital microscope. To ensure statistical reliability, multiple measurements were taken for each slot, and the average values were adopted as the final results [28]. Based on these data, the relationship between surface roughness and feed per tooth was plotted, as shown in Fig. 7.

As illustrated in Fig. 7, the surface roughness demonstrates a significant non-linear correlation with the feed per tooth. When the feed rate increases from 0.07 to $0.2 \mu\text{m}/\text{z}$, the surface roughness decreases from 0.14 to $0.08 \mu\text{m}$, corresponding to an improvement of 42.9%. However, a further increase in feed to $0.3 \mu\text{m}/\text{z}$ results in a rebound of the roughness to $0.13 \mu\text{m}$. This non-monotonic behaviour can be attributed to the size effect prevalent in micro-milling

processes. At lower feed rates, the ploughing effect induces plastic deformation and material accumulation, leading to elevated surface roughness. With increased feed, the mechanism shifts toward shear-dominated material removal, thereby enhancing surface quality. Beyond a critical feed threshold, exacerbated tool wear and dynamic instabilities contribute to the degradation of surface finish.

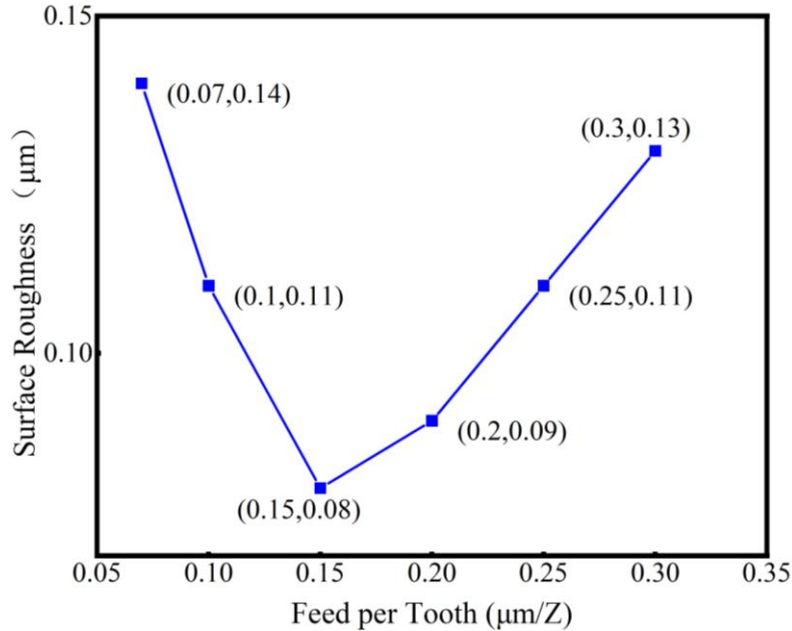


Figure 7: Surface roughness versus feed per tooth.

To achieve optimal surface integrity, it is essential to carefully control the feed per tooth within the recommended range of 0.15–0.2 $\mu\text{m}/\text{z}$. Within this region, the material removal process is governed predominantly by shearing, yielding superior surface quality with Ra values not exceeding 0.09 μm . Furthermore, to maximize machining performance, it is advised to synergistically optimize other cutting parameters such as cutting speed and depth of cut. Employing advanced tool coatings and high-pressure coolant strategies may also mitigate thermal effects and reduce tool wear. Finally, in-process monitoring techniques such as acoustic emission or force sensing can be incorporated to detect tool condition and process anomalies, facilitating adaptive control for consistent surface finish in industrial applications.

5. CONCLUSION

This study investigated the micro-milling process of T2 copper using a 1 mm diameter diamond end mill through an integrated approach combining numerical simulation and experimental validation. The systematic analysis of the influence of feed per tooth on cutting forces and surface roughness revealed that the detrimental effect of ploughing on surface quality significantly exceeds that of shear deformation, with ploughing-dominated mechanisms severely compromising surface integrity.

As the feed per tooth increased from 0.07 to 0.2 $\mu\text{m}/\text{z}$, surface roughness improved from 0.14 to 0.08 μm (a reduction of 42.9%), attributed to the transition in material removal mechanism from ploughing-dominated to shear-dominated regimes. However, further increasing the feed to 0.3 $\mu\text{m}/\text{z}$ resulted in a rebound in roughness to 0.13 μm , highlighting the dual influence of size effects in micro-milling: ploughing effects at low feed rates and tool wear at high feed rates collectively govern surface morphology evolution. Notably, the feed range of 0.15–0.2 $\mu\text{m}/\text{z}$ was identified as the optimal process window, where shear-dominated material removal achieves superior surface quality with $Ra \leq 0.09 \mu\text{m}$.

Critically, a transition point in material removal mechanism was observed at 0.22 $\mu\text{m}/\text{z}$, marking the shift from ploughing to shear deformation. When the feed exceeded 0.44 $\mu\text{m}/\text{z}$, ploughing was completely eliminated, and material removal occurred solely through slip-shear mechanisms, resulting in further improved surface quality. These findings provide a theoretical foundation for optimizing micro-milling parameters and enhancing surface integrity in precision manufacturing.

ACKNOWLEDGEMENT

This work was supported by the First Industry-Education Integration Project of Geely University of China (Grant No. 2025XOGY014). The authors are deeply grateful to Senior Engineer Liu Shougang from the ME Center of Geely Automobile Group for his professional guidance and valuable suggestions on research design and data analysis. His profound insights significantly enhanced the understanding of the research problem and improved the methodological framework of this study.

REFERENCES

- [1] Rathod, V. P.; Wankhade, S. H. (2025). A review on impact of micro-tools on micro-milling outcomes for aluminium alloy, *Advances in Science and Technology Research Journal*, Vol. 19, No. 3, 322-340, doi:[10.12913/22998624/200007](https://doi.org/10.12913/22998624/200007)
- [2] Mei, L.-F.; Liu, Y.; Yan, D.-B.; Yang, J.; Liang, Y., Luo, S.-M. (2024). Experimental study on magnetic field-assisted laser scanning welding of T2 copper, *Journal of Laser Applications*, Vol. 36, No. 1, Paper 012021, 14 pages, doi:[10.2351/7.0001245](https://doi.org/10.2351/7.0001245)
- [3] Mahmat, A.; Agar, S.; Tosun, N. (2025). Ultrasonic-assisted high-speed micro-milling of Ti6Al4V, *Journal of the Brazilian Society of Mechanical Sciences and Engineering*, Vol. 47, No. 1, Paper 46, 14 pages, doi:[10.1007/s40430-024-05334-7](https://doi.org/10.1007/s40430-024-05334-7)
- [4] Thepsonthi, T.; Özel, T. (2015). 3-D finite element process simulation of micro-end milling Ti-6Al-4V titanium alloy: experimental validations on chip flow and tool wear, *Journal of Materials Processing Technology*, Vol. 221, 128-145, doi:[10.1016/j.jmatprotec.2015.02.019](https://doi.org/10.1016/j.jmatprotec.2015.02.019)
- [5] Wang, F.; Zhao, J.; Li, A.; Zhao, J. (2014). Experimental study on cutting forces and surface integrity in high-speed side milling of Ti-6Al-4V titanium alloy, *Machining Science and Technology*, Vol. 18, No. 3, 448-463, doi:[10.1080/10910344.2014.926690](https://doi.org/10.1080/10910344.2014.926690)
- [6] Mayer, T.; Kieren-Ehse, S.; Willrich, M.; Kirsch, B.; Aurich, J. C. (2024). Wear behavior of all-ceramic micro end mills in micro milling of PMMA, *The International Journal of Advanced Manufacturing Technology*, Vol. 135, Nos. 1-2, 851-861, doi:[10.1007/s00170-024-14210-6](https://doi.org/10.1007/s00170-024-14210-6)
- [7] Chen, N.; Liu, J.; He, N.; Xiao, X.; Zhao, J.; Jia, Y.; Yu, N. (2024). Fabrication of high aspect ratio grooves on aluminium nitride by laser and chemical milling enhanced micro milling, *Journal of Materials Processing Technology*, Vol. 325, Paper 118299, 17 pages, doi:[10.1016/j.jmatprotec.2024.118299](https://doi.org/10.1016/j.jmatprotec.2024.118299)
- [8] Lu, X.; Xv, K.; Wang, X.; Cong, C.; Zeng, F.; Steven, Y. L. (2024). Modeling of laser-assisted micro-milling Inconel718, *Precision Engineering*, Vol. 88, 854-866, doi:[10.1016/j.precisioneng.2024.05.007](https://doi.org/10.1016/j.precisioneng.2024.05.007)
- [9] Wang, S.; Zhao, S.; Xu, R.; Huang, L.; Sun, Z. (2025). An investigation on subsurface generation in ultra-precision milling of nickel with multiscale crystal plasticity FE model, *Journal of Manufacturing Processes*, Vol. 141, 815-828, doi:[10.1016/j.jmapro.2025.03.027](https://doi.org/10.1016/j.jmapro.2025.03.027)
- [10] Ding, Y.; Li, Q.; Jia, R.; Chen, L.; Liu, B. (2025). Surface texturing on polycrystalline diamond compact cutter by nanosecond laser processing, *Advanced Engineering Materials*, Vol. 27, No. 4, Paper 2402204, 8 pages, doi:[10.1002/adem.202402204](https://doi.org/10.1002/adem.202402204)
- [11] Parthiban, R.; Natarajan, U.; Kumaravadeivel, A. (2025). Effect of material composition and machining parameters on surface quality and wear in CNC turning of AA7075 using Taguchi design, *Technical Gazette*, Vol. 32, No. 6, 2034-2047, doi:[10.17559/TV-20240613001771](https://doi.org/10.17559/TV-20240613001771)
- [12] Liu, Q.; Xu, J.; Wang, X.; Yu, H. (2021). Tool model building and research on cutting simulation experiment of Ti6Al4V, Xu, J.; Pandey, K. M. (Eds.), *Mechanical Engineering and Materials (ICMEM 2020)*, Vol. 100, Springer, Cham, 59-79, doi:[10.1007/978-3-030-68303-0_6](https://doi.org/10.1007/978-3-030-68303-0_6)

- [13] Lerher, T.; Grum, Z.; Motaln, M.; Zadavec, M. (2024). Wear simulation of the conveyor belt transfer chute using the DEM, *International Journal of Simulation Modelling*, Vol. 23, No. 1, 77-88, doi:[10.2507/IJSIMM23-1-673](https://doi.org/10.2507/IJSIMM23-1-673)
- [14] Ullah, I.; Akinlabi, E. T.; Songmene, V.; Kouam, J.; Sadeghifar, M. (2024). A multiscale finite element modeling for predicting the surface integrity induced by thermo-mechanical loads during high-speed milling of Ti-6Al-4V, *CIRP Journal of Manufacturing Science and Technology*, Vol. 52, 246-263, doi:[10.1016/j.cirpj.2024.06.003](https://doi.org/10.1016/j.cirpj.2024.06.003)
- [15] Wu, D.; Zhao, C. L.; Huang, C. L.; Luo, X. (2025). Micro-texture optimization for titanium cutting tools via simulation, *International Journal of Simulation Modelling*, Vol. 24, No. 2, 333-344, doi:[10.2507/IJSIMM24-2-CO7](https://doi.org/10.2507/IJSIMM24-2-CO7)
- [16] Özel, T.; Olleak, A.; Thepsonthi, T. (2017). Micro milling of titanium alloy Ti-6Al-4V: 3-D finite element modeling for prediction of chip flow and burr formation, *Production Engineering*, Vol. 11, Nos. 4-5, 435-444, doi:[10.1007/s11740-017-0761-4](https://doi.org/10.1007/s11740-017-0761-4)
- [17] Zębala, W.; Kowalczyk, R. (2015). Estimating the effect of cutting data on surface roughness and cutting force during WC-Co turning with PCD tool using Taguchi design and ANOVA analysis, *The International Journal of Advanced Manufacturing Technology*, Vol. 77, Nos. 9-12, 2241-2256, doi:[10.1007/s00170-014-6382-6](https://doi.org/10.1007/s00170-014-6382-6)
- [18] Hao, X.; Cui, W.; Li, L.; Li, H.; Khan, A. M.; He, N. (2018). Cutting performance of textured polycrystalline diamond tools with composite lyophilic/lyophobic wettabilities, *Journal of Materials Processing Technology*, Vol. 260, 1-8, doi:[10.1016/j.jmatprotec.2018.04.049](https://doi.org/10.1016/j.jmatprotec.2018.04.049)
- [19] Liang, M.; Wang, Y. (2020). Finite element study on chip morphology evolution of Ti6Al4V in micro-milling, *Journal of Physics: Conference Series*, Vol. 1633, Paper 012148, 6 pages, doi:[10.1088/1742-6596/1633/1/012148](https://doi.org/10.1088/1742-6596/1633/1/012148)
- [20] Gong, Q.; Wang, X.; Zhang, T.; Hou, X.; Shen, Z.; Liu, X. (2022). Warm laser shock micro-heading forming (T2 copper): numerical simulation and experimental research, *The International Journal of Advanced Manufacturing Technology*, Vol. 119, Nos. 3-4, 1491-1511, doi:[10.1007/s00170-021-08334-2](https://doi.org/10.1007/s00170-021-08334-2)
- [21] Yang, Z.; Lin, Y.; Liu, S.; Li, Y.; Dong, Y. (2018). Cutting force prediction models based on Box-Behnken design in high-speed milling of titanium alloy TC11, *Aviation Precision Manufacturing Technology*, Vol. 54, No. 4, 14-18
- [22] Li, L.; Yang, D. L.; Cui, Y. M. (2023). Optimization of machining performance in deep hole boring: a study on cutting tool vibration and dynamic vibration absorber design, *Advances in Production Engineering & Management*, Vol. 18, No. 3, 371-380, doi:[10.14743/apem2023.3.479](https://doi.org/10.14743/apem2023.3.479)
- [23] Li, A.; Zhao, J.; Zhou, Y.; Chen, X.; Wang, D. (2012). Experimental investigation on chip morphologies in high-speed dry milling of titanium alloy Ti-6Al-4V, *The International Journal of Advanced Manufacturing Technology*, Vol. 62, Nos. 9-12, 933-942, doi:[10.1007/s00170-011-3854-9](https://doi.org/10.1007/s00170-011-3854-9)
- [24] Fouathiya, A.; Meziani, S.; Sahli, M.; Barrière, T. (2021). Experimental investigation of microtextured cutting tool performance in titanium alloy via turning, *Journal of Manufacturing Processes*, Vol. 69, 33-46, doi:[10.1016/J.JMAPRO.2021.07.030](https://doi.org/10.1016/J.JMAPRO.2021.07.030)
- [25] Figueiredo, D.; Guimares, B.; Silva, T. E. F.; Fernandes, C. M.; Davim, J. P. (2025). An experimental study for ductile mode control on cemented carbide micro-milling, *International Journal of Refractory Metals and Hard Materials*, Vol. 129, Paper 107119, 12 pages, doi:[10.1016/j.jrmhm.2025.107119](https://doi.org/10.1016/j.jrmhm.2025.107119)
- [26] Amin, M.; Rathore, M. F.; Ahmed, A. A.; Saleem, W.; Li, Q.; Israr, A. (2023). A feed direction cutting force prediction model and analysis for ceramic matrix composites C/SiC based on rotary ultrasonic profile milling, *Advances in Production Engineering & Management*, Vol. 18, No. 3, 288-302, doi:[10.14743/apem2023.3.473](https://doi.org/10.14743/apem2023.3.473)
- [27] Sun, P. F.; Zhang, Y.; Wu, X. J.; Du, J. Y.; Hou, R. R.; Liu, J. (2024). Simulation and analysis of a preemptive transportation model using Flexsim software, *International Journal of Simulation Modelling*, Vol. 23, No. 2, 335-346, doi:[10.2507/IJSIMM23-2-CO7](https://doi.org/10.2507/IJSIMM23-2-CO7)
- [28] Yu, J. P.; Zou, D. Y.; Liu, X. A.; Zhang, Y. (2021). Simulation and experimental study on hybrid bit with different cutters, *International Journal of Simulation Modelling*, Vol. 20, No. 1, 87-98, doi:[10.2507/IJSIMM20-1-545](https://doi.org/10.2507/IJSIMM20-1-545)